ACS APPLIED MATERIALS & INTERFACES

Research Article

www.acsami.org

Novel Ultrathin Poly(ethylene glycol) Films as Flexible Platform for Biological Applications and Plasmonics

Nikolaus Meyerbröker,[†] Thomas Kriesche,[‡] and Michael Zharnikov*[,†]

[†]Angewandte Physikalische Chemie and [‡]Physikalisch Chemisches Institut, Universität Heidelberg, 69120 Heidelberg, Germany

ABSTRACT: We present a novel approach to prepare ultrathin, biocompatible films based on cross-linking of multi-functionalized, star-branched poly(ethylene glycols) (STAR-PEGs) with tunable film thicknesses of 4−200 nm. A two-component mixture of amine- and epoxy-terminated four-arm STAR-PEGs (M_N = 2000 g/mol) was spin-coated on a flat substrate. Gentle heating induced an extensive chemical cross-linking of the macromonomers, resulting in a stable, hydrogel-like film with a density close to that of bulk PEG material. The cross-linking process could be monitored in situ, exhibiting the expected kinetics. The films revealed pronounced swelling behavior, which was fully reversible and could be precisely controlled. Additionally, they provided a high affinity to citrate-stabilized gold nanoparticles (AuNP) that could be adsorbed with high densities into the PEG matrix from an aqueous solution. These novel PEG/AuNP composite films offer interesting and potentially useful optical properties. The adsorption could also be performed in a lithographic fashion, resulting in AuNP patterns imbedded into the PEG matrix.

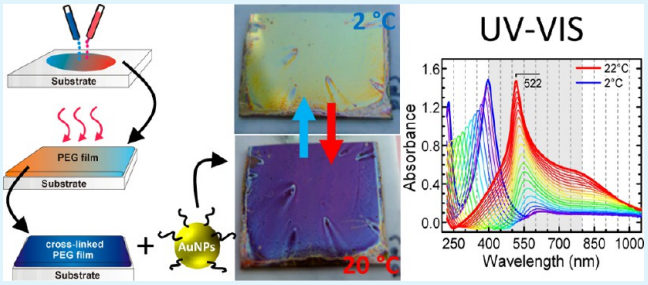

KEYWORDS: *biocompatibility, poly(ethylene glycols), hydrogel films, thermo-responsive swelling, nanoparticle-embedded polymer*

INTRODUCTION

Poly(ethylene glycol) (PEG) is a hydrophilic, synthetic polymer that has, despite the simple chemical structure, remarkable properties that makes it interesting for both scientific and commercial applications.[1] The most important feature of PEG is its biocompatibility − the material is non-toxic, resists unspecific protein adsorption[2,3] and cell adhesion,[4] as well as prevents the activation of immune cells,[5] which is the initial step in inflammation reaction.

Even at high molecular weights, PEGs are soluble in water[6] and, therefore, bulky PEG materials can exist in an aqueous environment only as a cross-linked polymer. Nevertheless, the PEG chains remain flexible to some extent and have a high affinity to water. Accordingly, depending on degree of cross-linking, the PEG network is able to adsorb reversibly a significant amounts of water, which is manifested by its spongy swelling.[7] Because such a swollen PEG material has a gel-like consistency, it is usually referred as PEG hydrogel.[8]

The properties of PEG, above all the biocompatibility, can be transferred to a particular object as far as stable PEG coating can be prepared.[9,10] Among other means, such coatings can be fabricated by immobilizing PEG chains chemically on the substrate surface. One way to do this is to attach appropriately functionalized PEG molecules to the substrate directly or over an intermediate coupling moiety immobilized on the substrate.[11−14] This so-called "grafting-to" method allows a good control over the character of coating but, especially for long PEG chains, the packing density of the resulting films is limited because of mutual sterical hindrance of the adjacent moieties.[14] High density (and order) can then only be achieved for comparably thin films, in particular for self-assembled monolayers (SAMs) of small, PEG-terminated molecules.[2,15,16] Alternatively, reasonably dense PEG coatings of variable thickness can be prepared by surface initiated polymerization (SIP) which is frequently referred to as "grafting-from" method.[17,18]

Further, PEG-modified surfaces can be obtained by applying a PEG oligomer on specially prepared substrates which are, in most cases, functionalized, providing a chemical coupling to the PEG film.[19−25] As starting material, acrylate-[19,20] or isocyanate-terminated[21−24] poly(ethylene glycols) are frequently used, whose chains can be linear[19,20] or branched (so called STAR-PEGs).[21−25] They are dissolved in a suitable solvent, placed on the substrate by drop or spin-casting, and subsequently cross-linked, which is the crucial step for the film stability. A cross-linking within the PEG film can be mediated by different means, including exposure to UV light[19,20,25] and a predefined chemical coupling.[21−24] In all cases, a special custom modification or design of the monomers and/or addition of further chemicals or cross-linking agents is required that restricts the versatility.

Alternatively to the chemically coupled PEG coatings, weakly attached films can be prepared and later separated from the substrate and used as biocompatible, hydrogel-like membranes.[26] Also in this case, cross-linking is mostly mediated

Received: January 7, 2013
Accepted: March 13, 2013
Published: March 13, 2013

by UV light exposure and specially designed monomers are required.

Here we present a novel, relatively simple and versatile route to prepare biocompatible PEG coatings on a broad variety of solid substrates. The procedure relies on commercially available compounds with no additional modification or functionalization and no utilization of UV treatment which can damage the PEG moieties to some extent.[27−29] The key idea is to mix two complementary components that polymerize spontaneously at a slightly elevated temperature. As such components, we used differently functionalized STAR-branched PEGs as shown in Figure 1. One of these PEG compounds carries nucleophilic

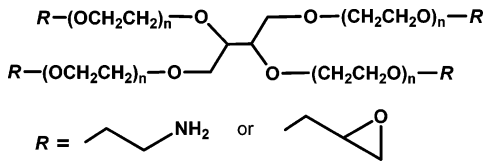

Figure 1. Chemical structure of amine- and epoxy-terminated, 4-arm STAR-PEGs (STAR2k-NH2 and STAR2k-EPX) as the basis for cross-linked and ultrathin PEG films.

functional groups, whereas the other one comprises electrophilic functionalities, promoting the intermolecular coupling. This design guarantees a very high degree of cross-linking, so that the films remained stable on nonfunctionalized, arbitrary substrates even after ultrasonication, and they can be potentially further processed into free-standing membranes. The thickness of the films could be precisely adjusted in a broad range. Along with biocompatibility, the films exhibited a variety of interesting and potentially useful properties as described below in this article.

EXPERIMENTAL SECTION

Preparation of PEG Films. Epoxy- and amino-terminated, four-arm polyethylene glycols with M_n = 2000 g/mol (abbreviated as STAR2k-EPX and STAR2k-NH2, respectively), purchased from Creative PEGWorks USA, were separately dissolved in chloroform with concentrations between 0.75 and 30 mg/mL. An equally concentrated 1:1 mixture of these two compounds was spin-coated (4000 rpm) on a 100 nm polycrystalline Au(111) substrate (Georg-Albert-PVD, Germany) which was preliminary cleaned under an ozone producing UV lamp for 15 min and rinsed with ethanol. Cross-linking of the PEG components was performed by gentle heating at 80 °C under argon atmosphere for 6 h followed by ultrasonication to remove non-cross-linked material. The resulted PEG films could be stored over months at −18 °C without notable degradation.

Infrared reflection absorption spectroscopy (IRRAS) measurements were performed under rough vacuum conditions (p < 1 mbar) using a Fourier transform IR spectrometer (IFS66v, Bruker) equipped with a liquid nitrogen-cooled MCT detector. The angle of incidence was fixed at 82°, and the spectra were recorded at a resolution of 2 cm^{-1} with an accumulation of 128 scans. As a reference, clean Au(111) substrate was used. The temperature of the samples could be varied up to 80°C by a computer-controlled Peltier plate mounted on the sample holder of the spectrometer.

Ellipsometry measurements were conducted with a spectroscopic ellipsometer (M-44, J.A. Woollam) at a fixed incidence angle of ∼75° and under ambient conditions. Film thicknesses were calculated by adapting the experimental data to a bilayer model consisting of the gold substrate and the PEG film. The optical constants for the substrate were determined using a clean gold surface, whereas those of the polymer film were obtained by using a Cauchy layer dispersion relation including the first two terms and adapting both coefficients to the ellipsometric measurement. Along with the primary characterization of the PEG films, ellipsometry was used to monitor the swelling properties. For this purpose, the films were placed on a home-build, computer-controlled Peltier plate, which allowed to vary the relative humidity experienced by these films in a controlled fashion. The ellipsometric analysis software (VWASE32, J.A. Woollam) made it possible to record the film thickness continuously, while decreasing the PEG film temperature with a rate of ∼0.1 °C/s.

X-ray photoelectron spectroscopy (XPS) measurements were carried out under UHV conditions with a MAX200 (Leybold-Heraeus) spectrometer equipped with an MgKα X-ray source and a hemispherical analyzer. The raw spectra were divided by the transmission function of the spectrometer and evaluated by a standard fitting procedure. The photoemission peaks were adapted to symmetrical Gaussian-Lorentzian product function with 80 % Gaussian proportion for the O 1s, C 1s, and N 1s emissions and 94 % for the Au 4f signal. A Shirley-type background was used.

The biocompatibility of the PEG films was examined by protein adsorption experiments. They were initially immersed into a PBS buffer solution for 30 min. Subsequently, a filtered, PBS-buffered solution of the test proteins, viz. fibrinogen or avidin, was added getting a total protein concentration of 0.25 mg/mL. After 60 min incubation time under ambient conditions, the PEG films were rinsed extensively with copious amounts of Milli-Q water. The amount of the adsorbed proteins was quantified by XPS, using the characteristic N 1s emission of the proteins. Note that this approach is quite sensitive to even small amounts of adsorbed proteins and frequently used for their monitoring.[30]

PEG/AuNP composite films were prepared by immersion of the PEG films into a freshly prepared (not older than 1 month; stored at 4 °C) solution of citrate-stabilized gold nanoparticles (AuNP) for 6 h, followed by extensive rinsing with water and drying in a nitrogen stream. The PEG/AuNP composite films could be stored for months at −18 °C without noticeable change in their properties. The citrate-stabilized AuNPs with a diameter of ∼15 nm were prepared by reduction of $AuCl_3$ according to well-establishes protocols.[31] In brief, 50 mg of $HAuCl_4{\cdot}3H_2O$ were dissolved in 150 mL of water and heated to boiling. Under vigorous stirring 150 mg of sodium citrate dissolved in 15 mL of water was added into the solution. The color changed from initially yellow to deep purple, indicating the formation of colloidal gold particles.

UV−vis spectra from the PEG/AuNP composite films were recorded in normal incidence geometry. As light source we used a deuterium-tungsten halogen lamp (DH-2000-BAL, Micropack GmbH) covering a spectral range of 190-2000 nm. The spectra were recorded with a grating spectrometer (HR2000, Ocean Optics) which covers a wavelength range of 200-1100 nm and provides an optical resolution better than 0.1 nm. For the measurements under swelling conditions, the temperature of the sample was varied by a computer-controlled Peltier plate with a rate of ∼0.1 °C/s.

Patterned PEG/AuNPs composite films were fabricated by electron beam lithography using poly(methyl methacrylate), PMMA, (50 kDa; 5 % in chlorobenzene, Allresist GmbH) as resist material. PMMA was spin-coated (4000 rpm) onto the PEG film and dried overnight under ambient conditions. Patterning was performed by an electron beam writer consisting of a scanning electron microscope (LEO 1530 Gemini, Zeiss) and a lithographic controller unit (Elphy Quantum, Raith GmbH) at p < 10^{-5} mbar. The energy of the electron beam was set to 20 keV and best results were obtained for 120-140 $\mu C/cm^2$ irradiation dose. Afterwards, the resist was developed in a 3:1 mixture of isopropanol (IPA) and methyl isobutyl ketone (MIBK) for 15 min followed by rinsing with IPA and drying under nitrogen atmosphere. The samples were subsequently immersed for 1 h into the AuNP solution and, finally, the resist was removed by acetone. Both homogeneous and patterned PEG/AuNPs composite films were imaged by secondary electron microscopy (SEM). For optical or UV lithography, AuNP/PEG composite films were first sprayed with a photo-sensitive resist (Positiv20, Kontakt Chemie). The sample was then illuminated with a white lamp light (100 W) through a grid for 30 min, and the resulting pattern was developed in a 0.8 % NaOH solution for 2 min and rinsed with water. Afterwards, the pattern was

Scheme 1. Schematic Representation of the Preparation Procedure: (a) Spin-Coating of the Mixed Solution of Both PEG Macromers on a Flat, Solid Substrate, (b) Cross-Linking of the PEG Macromers at Elevated Temperature, and (c) the Removal of Unreacted PEG Macromers by Washing or Ultrasonication

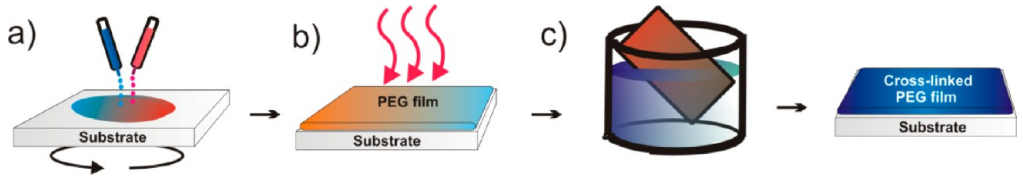

immersed into a 1% KI/I2 solution for 15 s to dissolve the AuNPs in the irradiated regions. Finally, the residual resist was removed by acetone.

RESULTS AND DISCUSSION

General Procedure. The general procedure for the preparation of highly cross-linked PEG films is schematically presented in Scheme 1. As mentioned above, we used a two-component system of differently functionalized multi-functional PEG oligomers (Figure 1). One component carried nucleophilic amino groups (STAR2k-EXP), whereas the other one had complementary electrophilic epoxide moieties (STAR2k-NH2). Both components were separately dissolved in chloroform at the same concentration varied from 0.75 to 30 mg/mL, mixed with one another in relation 1:1, and spin coated on Au(111) substrate. Afterwards the STAR2k-EXP and STAR2k-NH2 monomers were cross-linked thermally and extensively rinsed with water or ultrasonicated in water to remove non-bound and weakly bound species.

IRRAS. The intermolecular cross-linking was mediated by the thermally initiated chemical reaction between the terminal epoxy groups of STAR2k-EXP and the amino moieties of STAR2k-NH2. This process was monitored in situ by IRRAS when mounting the spin-coated PEG film on a computer-controlled Peltier plate in the vacuum chamber of the IR spectrometer. The individual spectra of STAR2k-EPX and STAR2k-NH2 recorded at ambient temperature are shown in Figure 2a; they exhibit the typical IR vibration pattern of amorphous polyethylene glycols.[15,32] Both spectra are hardly distinguishable, which is not surprising since the molecules are very similar and only differ by the terminal functional groups. Nevertheless, the symmetrical C−O stretching vibration of the epoxy group could be clearly identified at 913 cm^{-1} exclusively in the spectrum of the STAR2k-EPX (grey shaded area in Figure 2a). This band could then be used to monitor the cross-linking reaction in the STAR2k-EXP/STAR2k-NH2 film because this reaction involves the ring-opening of the epoxy group resulting in a disappearance of the respective C−O stretching vibration.

Along these lines, the film was heated to 80°C and kept at this temperature to promote the cross-linking while IR spectra were recorded continually to monitor the reaction of STAR2k-NH2 and STAR2k-EXP. In Figure 2b, the spectra of the epoxy band region are presented for three selected time points. They show that the vibration decreases in intensity continuously in the course of the reaction and vanishes almost entirely after 180 min.

Taking the intensity of the C−O stretching vibration of the epoxy group as a measure of the amount of the STAR2k-EXP reactant, the order of the cross-linking reaction can be precisely determined on the basis of the standard rate laws. Plotting the reciprocal intensity of the epoxy band ($1/c$) against the reaction

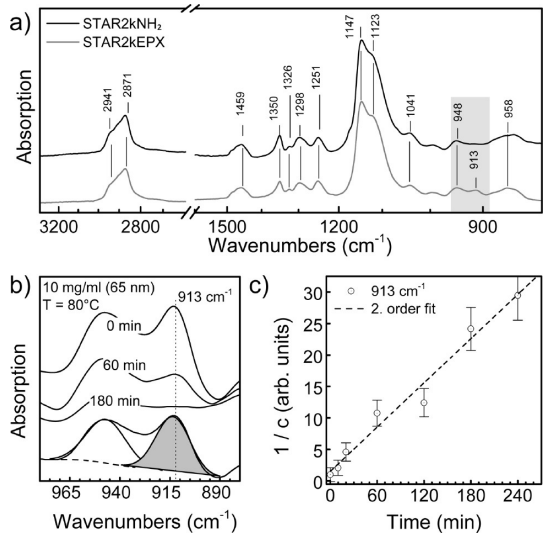

Figure 2. (a) IRRAS spectra of STAR2k-NH2 (black line) and STAR2k-EXP (grey line) compounds; the shaded region highlights the C−O stretching band of the epoxy ring. (b) Detailed spectra of the epoxy band region acquired in the course of cross-linking reaction of STAR2k-NH2 and STAR2k-EXP; the intensity of the band is obtained by fitting the signal to a Lorentz function (dark shaded peak in the bottom spectrum). (c) Inverse intensity of the epoxy band plotted as a function of the reaction time.

time t, the points can be adapted to a straight line, indicating a second order reaction for the opening of the epoxy ring (Figure 2c). Such a rate law corresponds exactly to our expectation for the cross-linking reaction of STAR2k-EXP and STAR2k-NH2 and suggests that the epoxide group did not suffer from thermal degradation which would correspond to a first-order kinetics. Note that the slope of the straight line in Figure 2c gives the second-order rate constant k_2 = 0.13 min^{-1} at a reaction temperature of 80 °C.

Ellipsometry is an easy and precise technique to monitor the thickness of the PEG films, which, as follows from the experimental data (see below), could be adjusted just by a specific choice of the PEG concentration in solution. The film thickness was determined twice: first after the spin coating, d_1, (step a in Scheme 1) and, again, after ultrasonication, d_2, (step (c) in Scheme 1). The logarithmic plots in Figure 3a give almost linear relationships between the concentration of the PEG mixture and the values d_1 and d_2 and imply the broad range of accessible film thicknesses between few and hundreds of nanometers.

The difference between d_1 and d_2 is plotted in Figure 3b. It is a measure of the material loss during the last step of the preparation procedure. However, at the same time, this parameter can be interpreted as a fingerprint of the film stability. This difference of 2-3 nm is nearly independent of the

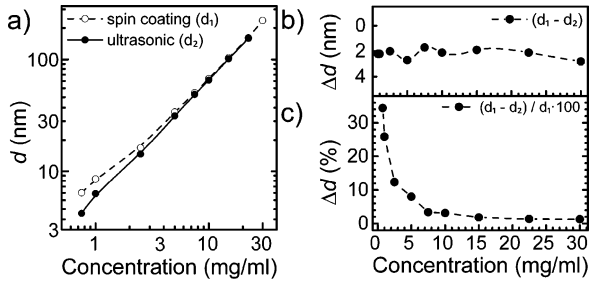

Figure 3. (a) Thickness of the PEG films after the spin-coating (open circles) and ultrasonication (filled circles) as a function of the concentration in the primary STAR2k-NH2 and STAR2k-EXP solution. (b) Absolute and (c) relative material loss upon ultrasonication.

concentration. Such a small loss of the layer thickness after ultrasonication is a clear indication of a highly efficient cross-linking within the PEG layer during the preparation process. Without a thermally-induced cross-linking, the films were almost completely removable just by gentle rinsing. Note that this material loss is exclusively related to the ultrasonication step since no noticeable decrease in the film thickness was observed upon the thermal treatment (cross-linking) step.

In contrast, the relative loss of the layer thickness upon ultrasonication exhibits significant dependence on the concentration as shown in Figure 3c. At low concentrations, corresponding to the small film thicknesses, it is much higher than that at high concentrations (thicker films), manifesting a lesser degree of the cross-linking in the former case. This suggests that the cross-linking reaction in the given case is only fully efficient at a sufficient concentration of the reactants.

XPS. The chemical composition and integrity of the PEG films were investigated by XPS. The wide range spectrum of a representative 20 nm film in Figure 4a exhibits the characteristic emissions of carbon (C 1s) and oxygen (O 1s), which are the major constituents of poly(ethylene glycols). In addition, there is an Au 4f signal from the gold substrate, which is only observed for the thin PEG films ($\leq$ 20 nm) but is not visible for distinctly thicker films due to the attenuation of the photoelectron signal. The nitrogen N 1s spectra exhibit a single emission at ~400.5 eV related to the amino groups of the STAR2k-NH2 moieties after the cross-linking reaction. This emission is quite weak due to the low nitrogen content in the film. Consequently, the N 1s spectra were not further considered except for the biocompatibility analysis (see below) because no deeper information could be extracted from them. Furthermore, no signals from contamination were observed suggesting a high purity of the PEG films.

The easy control over the film thickness by the concentration of the PEG solution made it possible to examine the dependence of the photoelectron signal intensities on the film thickness. A typical Au 4f spectrum and the respective results for the Au 4f intensity are presented in Figures 4b. This intensity exhibits an exponential attenuation with increasing film thickness d as it can be expected for the signal from a substrate, which is attenuated by an overlayer. The experimental curve can be adapted to a standard exponential decay function of the type $\exp(-d/\lambda_{Au4f})$,[33] where λ_{Au4f} is the attenuation length of the photoelectrons in the PEG film. The attenuation length is generally dependent on the kinetic energy of the photoelectrons and was estimated at 5.0 ($\pm$ 0.3) nm for the Au 4f photoelectrons in the given case. In contrast to the

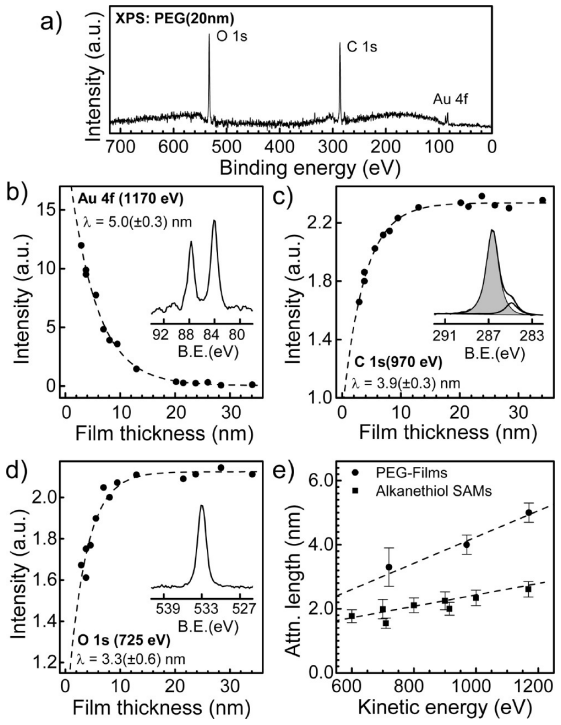

Figure 4. (a) Wide scan XPS spectrum of a 20 nm PEG film; the most pronounced emissions are marked. (b–d) Intensities of the (b) Au 4f, (c) C 1s, and (d) O 1s signals as functions of the ellipsometric film thickness, along with the theoretical fits by an exponential function; the kinetic energies of the photoelectrons and the derived values of the attenuation length are given in the plots; the respective narrow scan spectra are shown as insets. (e) Dependence of the attenuation lengths of the photoelectrons on their kinetic energy for the PEG films (filled circles) and reference alkanethiol SAMs (filled squares).

substrate's signal, the C 1s and O 1s intensities of the PEG films increase with the growing film thickness, since these photoelectrons were generated in the film itself (Figure 4c, d). However, because of the self-attenuation, the intensities do not rise to infinity but exhibit a saturation described by a standard function $1 - \exp(-d/\lambda)$.[33] The experimental curves for the intensities of the C 1s and O 1s emissions are fitted by this expression, resulting in attenuation lengths of λ_{C1s} = 3.9 ($\pm$ 0.3) nm and λ_{O1s} = 3.3 ($\pm$ 0.6) nm, respectively. These values as well as the value for the Au 4f emission are plotted in Figure 4e against the kinetic energy of the photoelectrons and compared to the corresponding attenuation lengths obtained for a series of well-defined alkanethiol self-assembled monolayers (SAMs). For the PEG films, the attenuation lengths are distinctly higher, which is presumably related to a lower specific density. Seah and Dench have described an empirical relationship between the specific density ρ of an organic film (in g/cm^3) and the attenuation length λ (in nm) of an arbitrary emission with the kinetic energy E (in eV)[34]

$$\lambda(E) = 1/\rho[49/E^2 + 0.11\sqrt{(E)}] \quad (1)$$

Using this formula and the attenuation lengths for the PEG films, their specific density was calculated as 0.84 ($\pm$ 0.1) g/cm. This is, indeed, lower than the analogous value for bulk poly(ethylene glycols), having a density of ~1.1 g/cm^3. Note, however, that the attenuation lengths used here for the density evaluation were determined on the basis of the PEG films with a thickness of less than 20 nm, which, in view of the comparably

lower degree of cross-linking in these films (see above), means that the value of 0.84 g/cm^3 is a lower limit. The density of the thicker PEG films, which have a higher degree of cross-linking, should be presumably higher, approaching the value for bulk PEG materials. Regretfully, the evaluation of the XPS data for these films is not possible because of the saturation of all the relevant photoemission signals.

Protein repelling properties or biocompatibility of the PEG films was tested by protein adsorption experiments. For this purpose, the films were incubated in a buffered protein solution, rinsed with distilled water to remove loosely bound proteins, and characterized by XPS using the specific N 1s signal to evaluate the amount of remaining, strongly bound proteins. It must be noted that the PEG films of this study have a low intrinsic amount of nitrogen because of the amino groups. This intrinsic amount must be taken into consideration, particularly at a low coverage of adsorbed proteins. As test proteins we used fibrinogen (340 kDa) and avidin (68 kDa), which are frequently used for this purpose since they show a strong tendency to adsorb on surfaces, with distinctly higher adsorption affinity in the case of fibrinogen. N 1s XPS spectra taken after adsorption of fibrinogen or avidin on either a clean gold substrate (reference, shaded grey) or on the substrate coated with a 10 nm (solid lines) or a 50 nm (dashed lines) PEG film are shown in panels a and b in Figure 5. The coating

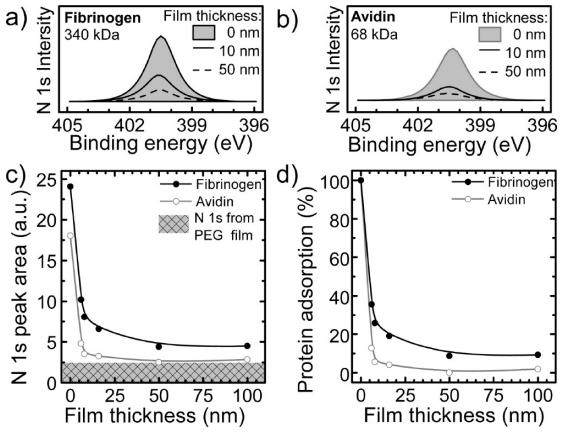

Figure 5. Biocompatibility of the PEG films proven by the protein adsorption experiments using fibrinogen and avidin as test proteins: N 1s XPS spectra taken after adsorption of (a) fibrinogen or (b) avidin on either the pristine substrate (shaded grey; reference for 0 nm PEG coating) or on the substrate coated with 10 nm (solid line) or 50 nm (dashed line) PEG film; (c) N 1s intensity plotted against the PEG layer thickness for the case of fibrinogen (filled circles) or avidin (open circles) adsorption (hatched area indicates the intrinsic nitrogen signal associated with the PEG films); (d) normalized protein content for the case of fibrinogen (filled circles) and avidin (open circles) adsorption to estimate the biocompatibility.

reduced significantly the amount of the adsorbed proteins (given by the additional intensity of the N 1s emission), with a larger effect for the thicker PEG film. This behavior becomes clearer when the intensities of the N 1s signals after the protein adsorption and subsequent rinsing are plotted against the thicknesses of the PEG films (Figure 5c). A strong decrease in the N 1s intensity with increasing thickness of the PEG coating is observed. The intensity values had, however, to be corrected for the inherent nitrogen content of the PEG films highlighted by the hatched area in Figure 5c. The curves obtained after this correction and normalization to the maximum adsorption on the reference surface (clean Au) are shown in Figure 5d; they are representative of the biocompatibility of the PEG films. As follows from these curves, the amount of the adsorbed fibrinogen is always larger than that of avidin in agreement with the higher affinity and larger size of the former protein. Further, similar to the curves in Figure 5c, a strong decrease in the amount of the adsorbed proteins with increasing thickness of the PEG coating is observed, so that the PEG films with a thickness exceeding 20 nm are almost fully resistant to the absorption of avidin whereas a small amount of fibrinogen is still observed. Presumably, this residual amount corresponds to the moieties trapped physically in the PEG matrix. It should require then a more extensive or prolonged rinsing to remove them from the matrix.

Note that the relatively high extent of the protein adsorption at the small thicknesses does not necessary means a poor biocompatibility but can be mostly related to the protein adsorption at the PEG/Au interface. The hydrogel-like nature of the PEG films makes possible a penetration of proteins into the film and their subsequent diffusion to the PEG/Au interface where they can be trapped even after the removal of the sample from the protein solution. The respective N1s signal will then be well perceptible at a small film thickness, making a wrong impression regarding the biocompatibility. This signal will decrease exponentially with increasing film thickness, which is exactly the behavior we observe in panels c and d in Figure 5.

Thermosensitive Swelling. The hydrogel-like nature of the PEG films was exhibited by their swelling behavior. In the case of thin films, such a behavior manifests itself as a thickness increase[35] occurring within a short response time.[36] To test this, we placed the samples on a temperature-controlling Peltier plate to vary the relative humidity above the film surface, which allowed us to precisely adjust the amount of water accumulated by the films. The swelling of the PEG films was recorded continually by ellipsometry. The thickness variation during multiple swelling steps as response to the temperature variation is shown in Figure 6a. The test PEG film had under ambient conditions (T_A = 22 °C and a relative humidity, r_h = 21 %) a thickness of 100 nm. This thickness did not change with increasing temperature, which means that the film has initially stored no water. However, if the temperature was lowered, the film started to swell gradually, following the changes in the relative humidity. At T =15 °C, the layer thickness was already 110 nm and, upon step-like temperature lowering down to ~2 °C, the film reached a maximum thickness of nearly 200 nm (Figure 6a). Note that a further temperature decrease did not lead to a further swelling but to the condensation of water droplets on the surface of the film.

The observed swelling behavior was completely reversible, and the film reacted instantaneously to the temperature changes on a time scale of one second. Plotting the thickness against the temperature and applying an offset, δ, of 2 °C, the curves shown in Figure 6b were obtained for the PEG films of different thicknesses. The temperature dependent thickness could be described by a general equation

$$d(T') = A + B\cdot\exp(-T'/k) \quad (2)$$

with $T' = T - \delta$ and the parameters A, B, and k describing the swelling properties of the PEG films. A represents the film thickness in the non-swollen, anhydrous state, i.e. at high temperature, while B corresponds to the additional film thickness due to swelling. The sum $A + B$ is the maximum

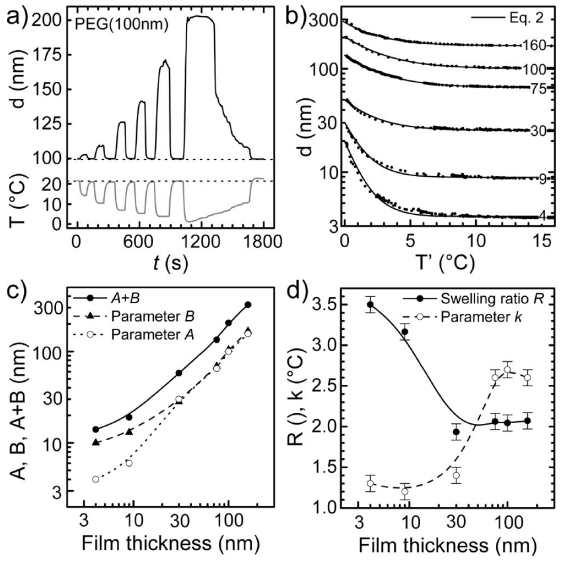

Figure 6. Swelling properties of the PEG films proven by adsorption of moisture while cooling on a Peltier plate: (a) thickness variation during multiple swelling steps of a 100 nm PEG layer (top curve) as response to the temperature variation (bottom curve); (b) thickness of the PEG films as a function of temperature for the films of different thicknesses in the non-swollen state (marked at the respective curves); the experimental data (black dots) can be fitted to an exponential decay function according to eq 2 (black lines); (c) dependence of the parameters A (open circles; dotted line) and B (filled triangles; dashed line) from eq 2 as well as their sum (filled circles; solid line) on the thickness of the PEG films; (d) dependence of the parameter k (open circles; dashed line) from eq 2 as well as the swelling ratio, $(A+B)/A$, (filled circles; solid line) on the thickness of the PEG films.

film thickness, i.e., the film thickness at $T' = 0$ °C, and the ratio of $A + B$ to A can be defined as the swelling ratio R, whereas $1/k$ reflects how sensitive the film is to temperature changes. The dependences of A, B and their sum on the layer thickness are plotted in Figure 6c, whereas the analogous dependences for k and the swelling ratio R are depicted in Figure 6d. The curves for A and B overlap practically at $d > 35$ nm, which means that the film thickness is doubled as reflected by the value of $R \approx 2$ in Figure 6d. For the thinner films, the value of B exceeds that of A, as reflected by the behavior of the swelling ratio which increases steadily with decreasing thickness at $d < 35$ nm, reaching ~3.5 for the thinnest PEG film. Note that the swelling ratio of hydrogels is generally dependent on the degree of their cross-linking. The lower the degree is, the higher the swelling ratio. This means that the maximum cross-linkage is only reached for the PEG films with a thickness of more than 30−35 nm, whereas the thinner films exhibit a progressively lower degree of cross-linking. This result agrees well with the conclusion made on the basis of the material loss data (Figure 3c). The thinnest films lose the most material in the ultrasonication process due to incomplete cross-linking, and exhibit the highest swelling ratio, accordingly. Starting from a thickness of 30−35 nm, the material loss is constant and relatively small (> 5%; see Figure 3c), which corresponds to the films exhibiting moderate and thickness-independent swelling.

PEG/AuNP Composite Films. Because of the pronounced swelling properties, the PEG films are capable to adsorb individual objects dissolved in aqueous solutions. In this context, the behavior of colloidal gold (gold nanoparticles, abbreviated hereinafter as AuNPs) was investigated. Because of the citrate shell (see Experimental Section), these particles were potentially capable to bind to the PEG moieties and form a novel PEG/AuNP composite. Since the penetration started from the film−solution interface, most of the particles were located at this interface or in its vicinity, preventing the penetration of further AuNPs; an indirect evidence for this behavior will be provided in the next section.

After the immersion of the PEG films into an aqueous solution of AuNPs (~15 nm diameter), a clear change in the optical appearance of the films was observed. Depending on the film thickness in non-swollen state and duration of immersion, the initially colorless and transparent PEG films became colored purple or green (Figure 7a, b). The most likely

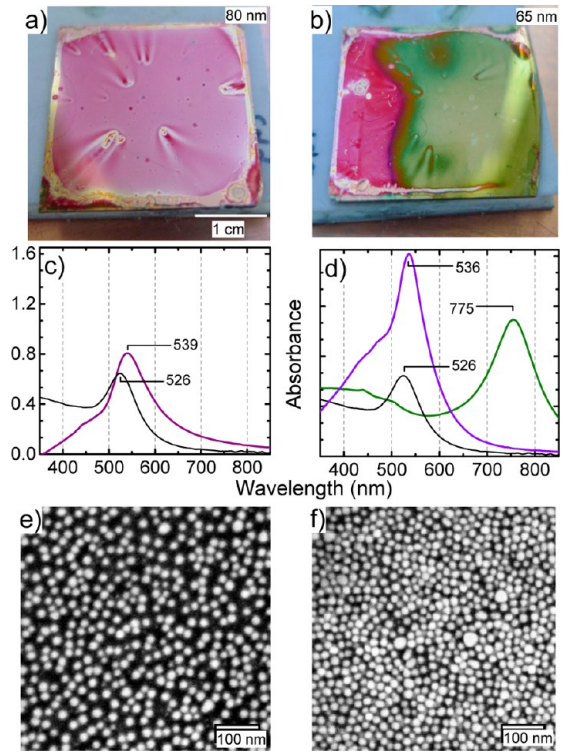

Figure 7. (a, b) Optical images of two PEG/AuNP composite films immersed in the AuNP solution for different time; in the case of (b), the immersion time was different for the left and right parts, being similar to *a* and shorter for the left area; (c, d) corresponding UV-VIS spectra (colored lines) acquired, in the case of *b*, from the different areas of the film (color coded), along with the spectrum of the saturated, aqueous solution of AuNPs (grey lines); (e) SEM image of the film in *a*, which is also characteristic of the purple-colored area of the film in *b*; (f) SEM image of the green-colored area of the film in *b*.

explanation for this behavior is the excitation of the local surface plasmon resonance (LSPR) in AuNPs, similar to the saturated aqueous solution of these moieties which is colored purple by the LSPR excitation in the visible range. Indeed, as shown in panels c and d in Figure 7, the UV−vis spectra of some PEG/AuNP composite films are similar to the spectra of the aqueous AuNP solution. This applies primarily to the purple films (Figure 7a and Figure 7b, left area). However, some composite films are green (Figure 7b, right area), which means a significant red shift of the LSPR band (Figure 7d, green curve). It is well known that the position of the plasmon resonance is affected by the shape and size of the AuNPs as well as by the dielectric properties of the surrounding medium.[37]

However this cannot explain a large red shift of more than 200 nm. The answer is given by the SEM images of the films presented in images e and f in Figure 7. According to these images, the packing density of AuNPs in the purple films with 1.1×10^{11} cm^{-2} (Figure 7a and left part of Figure 7b) is much lower than that in the green film with 2.5×10^{11} cm^{-2} (Figure 7b, right part). Thus, the interparticle spacing of the embedded AuNPs is much smaller in the latter case. It is however known that if such spacing is in the range of the particle diameter or lower, the AuNPs may no longer be considered as individual objects (as, for example, in the aqueous solution) but behave in a collective fashion, which leads exactly to the observed red shift.[37−39] Significantly, even at a small interparticle spacing, AuNPs were not agglomerated in our case but well-separated from one another, which can be tentatively explained by repelling interaction between the negatively charged citrate shells.

Swelling of the PEG/AuNP Composite Films. The color of the composite films as well as the positions of the LSPR absorption band can be explained qualitatively on the basis of the AuNP spacing. Another important feature, which was observed in parallel, was the relatively high intensity of this band as follows from the comparison of the spectra of the monolayer-thin, composite films with that of the bulk AuNP solution (Figure 7c, d). Moreover, the composite films exhibited a significant change in the intensity of the LSPR band depending on their parameters as shown in Figure 7d. The latter effect was found to be especially strong upon the swelling of the PEG/AuNP composite films as shown in Figure 8 where the optical effect of the water drop on a test composite film (Figure 8a) and optical images of this film taken at 22°C and 2°C (Figure 8b) along with the UV/Vis spectra taken in the course of the cooling-induced swelling (Figure 8c) are presented. The film appeared deep blue in the nonswollen state, but became nearly transparent upon the swelling, either underneath the water drop (Figure 8a) or as a result of cooling

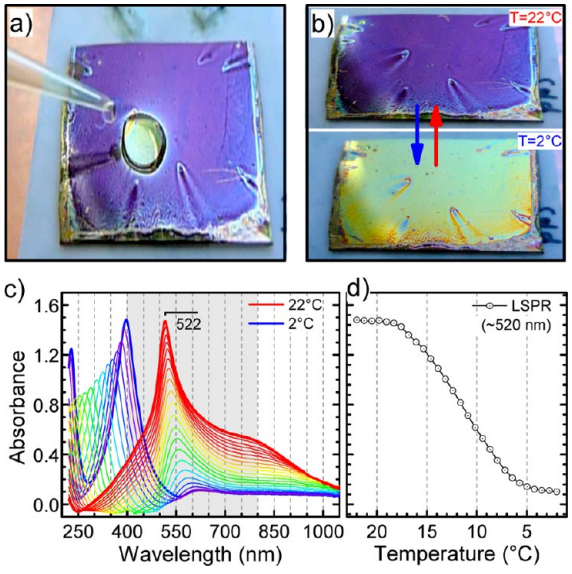

Figure 8. Influence of (a) a water droplet and (b) temperature-induced swelling on the optical appearance of the PEG/AuNP composite films; (c) consecutive UV−vis spectra acquired in the course of temperature-induced swelling; (d) strong decrease in the intensity of the LSPR band as a function of temperature, i.e., the extent of swelling.

(Figure 8b). This effect can be understood in detail by looking at the UV/Vis spectra taken in the course of swelling (Figure 8c). These spectra can be subdivided in two parts, viz. the UV and visible ranges. In the visible range, between 400 and 800 nm, the LSPR resonance is clearly visible at 522 nm at room temperature (non-swollen state). Its intensity decreases strongly with decreasing temperature (progressive swelling) and the band shifts slightly by ∼20 nm to longer wavelengths. The respective dependence of the maximum absorbance on the temperature is given in Figure 8d. It drops by about 1.5 absorbance units, which corresponds to a decrease in the intensity by a factor of 30. The UV range, between 220 and 400 nm, is characterized by interference bands whose positions and number depend on the film thickness. Accordingly, these bands change gradually both in intensity and position upon the film swelling.

The behavior of the LSPR band in the visible range can be tentatively explained as far as an interaction between the AuNPs and conductive gold substrate is taken into account, assuming that most of the AuNPs are located at and close to the film-ambience interface. A basically similar system has been studied theoretically and experimentally by others.[40−42] The system consisted of a metal substrate covered by a nanometer-thick, inorganic dielectric film that, in its turn, was covered by an assembly of isolated Au and Ag islands, analogous to the AuNPs of our study. It was found that there is only a slight shift of the LSPR band when changing the distance between the metal film and the metal islands. However, at the same time, a strong change in the intensity of the LSPR absorption in dependence on the thickness of the separation layer was observed. Initially, the intensity of the LSPR band increased to some extent with increasing thickness of the dielectric layer and reached a maximum at a thickness of ∼50 nm. However, with the further increase in the spacing between the nanoparticles and the metal film, the intensity decreased steeply. Exactly this behavior was observed in our case upon the swelling of the PEG/AuNP composite films, suggesting that our assumption about the inhomogeneous distribution of AuNPs in the PEG film is correct.

Lithographic Deposition of AuNPs into the PEG Matrix. Along with the laterally homogeneous embedding of AuNP into the PEG films, patterned deposition of these moieties was tested based on standard lithographic techniques. For micro- and nano structuring, the PEG films were coated with an electron-sensitive resist (PMMA), patterned by EBL, developed, and subjected to the AuNP solution, after which the residual resist was dissolved in a suitable solvent (see Experimental Section for details). A special care was taken when selecting the irradiation dose to keep the electron-beam-induced modification within the resist layer and to avoid a damage of the underlying PEG film which is prone to such damage[30] and can then lose its swelling properties. On the other hand, the dose was sufficiently high to ensure that the irradiated resist could be dissolved completely in the development step. The proof was a high density of the imbedded particles in the processed areas, close to the values observed for the homogeneous deposition. As a representative example, SEM images of an AuNPs pattern imbedded in a 70 nm PEG film are presented in Figure 9a−c, at several different magnifications and inverse contrast in the latter figure. The square areas containing AuNPs are well-defined and appear bright in Figure 9a. At high magnification, the individual particles are clearly visible as shown in images b and c in Figure

dx.doi.org/10.1021/am400065f | ACS Appl. Mater. Interfaces 2013, 5, 2641−2649

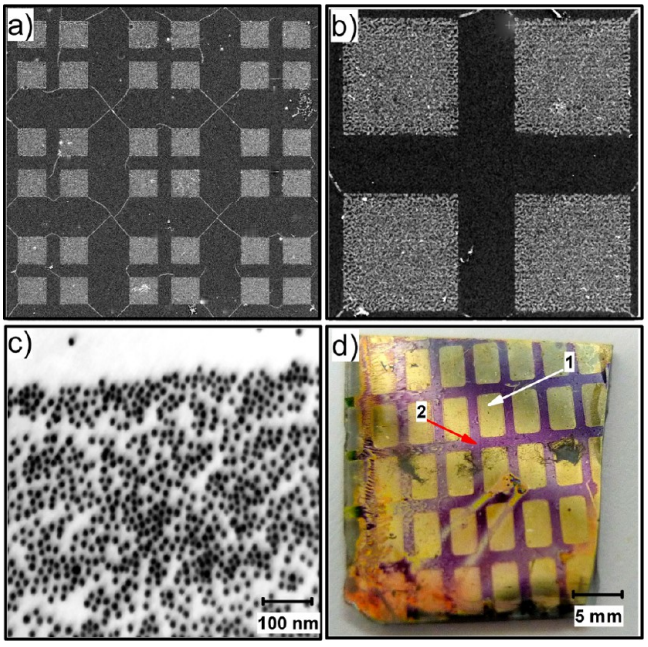

Figure 9. (a–c) SEM images of an AuNPs pattern embedded in a 70 nm PEG film taken at different magnifications; the contrast is inverse in *c*, so that AuNPs appear dark in this image. The pattern was prepared by EBL using PMMA as resist. (d) optical image of a patterned PEG/AuNPs composite film. The patterning was performed by optical lithography using a commercial resist. The areas exposed to the etching solution (marked by 1) appear yellow (the PEG film is transparent); the nonexposed ones (2) appear violet.

9. There density is sufficiently high and the contrast between the exposed and unexposed areas is high as well, with almost no adsorbed AuNPs in the latter areas.

Along with EBL, UV or optical lithography could be applied. In this framework, as a test experiment, a PEG/AuNP composite film was coated with a photoresist and exposed through a mesh to the light from a halogen lamp. After the development, the patterned PEG/AuNP film was exposed to a gold etching solution. As a result, AuNPs in the exposed areas were dissolved, whereas those in the non-exposed areas were still protected by the resist. After the removal of the resist with a suitable solvent, the pattern shown in Figure 9d was fabricated. The regions exposed to the light and, consequently, to the etching solution appear yellow, which is the color of the gold substrate covered by the transparent PEG film, whereas the nonexposed regions appear purple because of the optical effects related to the PEG/AuNP composite film (see previous sections).

CONCLUSIONS

We described here a novel approach to prepare ultrathin PEG films on a broad variety of solid substrates. The key idea of the approach is to mix two complementary components which polymerize at an elevated temperature after their deposition by spin-coating or another casting approach. As such components, we used amine- and epoxy-functionalized STAR-branched PEGs, which are commercially available. The polymerization required neither any additional modification of these compounds nor addition of any further chemicals or UV treatment which is frequently used for such purpose. This makes the procedure simple and reliable, in addition to its potential versatility in terms of the substrate.

The complementary nucleophilic (amino) and electrophilic (epoxy) functionalities of the STAR-branched PEGs promoted the efficient intermolecular coupling, resulting in a very high degree of cross-linking, so that the films remained stable even upon ultrasonication, exhibiting a material loss of 2–3% only. The thickness of the films could be precisely adjusted in a range of 4–200 nm by varying the concentration of the STAR-PEG compounds in the primary solution. Most important, the films exhibited high degree of biocompatibility as far as their thickness exceeded 20 nm and, probably, even at lower thicknesses but this could not be non-equivocally proved yet.

As expected for this class of materials, the PEG films revealed distinct hydrogel properties, demonstrating well-controlled and reversible swelling upon the variation of relative humidity or immersion in an aqueous solution. The films were found to be capable to adsorb individual objects dissolved in such solutions. This was demonstrated by the fabrication of high-density PEG/AuNP composites in which AuNPs were not agglomerated but well-separated from each other. These composite films exhibited interesting optical properties, explained by the LSPR excitation. We demonstrated that these properties change noticeably upon the variation of the AuNP density and degree of swelling which, in its turn, depends on the relative humidity. This behavior makes the PEG/AuNP composite films potentially useful for sensor fabrication, especially in view of the fact that AuNPs can be adsorbed lithographically, as was demonstrated in the present study.

Apart from the above potential application, the PEG films of this study can be used for more sophisticated lithography, providing, for example, a platform for biocompatibility patterns. They can also be probably used as hydrophilic and biocompatible coatings for contact lenses, since they fulfill the basic requirements for such coatings. Further, the PEG films can be potentially separated from the substrate and used as free-standing membranes or biocompatible support films. Such support films can be of interest for transmission electron microscopy (TEM) in its specific application to sensitive biological objects. Alternatively, the PEG films of this study can probably not only serve as a support film but also as ultrathin matrix layers in a TEM experiment, taking the studying nano-objects in their inner. These issues are currently under research in our lab and will be specifically addressed in forthcoming publications.

AUTHOR INFORMATION

Corresponding Author

*Corresponding Author Phone: +49 6221 544921. Fax: +49 6221 54 6199 E-Mail: Michael.Zharnikov@urz.uni-heidelberg.de.

Notes

The authors declare no competing financial interest.

ACKNOWLEDGMENTS

We thank Dr. W. Eck for the initiation of this project and Prof. M. Grunze for the support. This work has been supported by the Volkswagen Stiftung (83227) and DFG (Ec 152/4-1).

REFERENCES

(1) Greenwald, R. B. *J. Controlled Release* **2001**, *74*, 159–171.
(2) Prime, K. L.; Whitesides, G. M. *J. Am. Chem. Soc.* **1993**, *115*, 10714–10721.
(3) Li, L. Y.; Chen, S. F.; Zheng, J.; Ratner, B. D.; Jiang, S. Y. *J. Phys. Chem. B* **2005**, *109*, 2934–2941.

(4) Christophis, C.; Grunze, M.; Rosenhahn, A. *Phys. Chem. Chem. Phys.* **2010**, *12*, 4498−4504.
(5) Shen, M. C.; Martinson, L.; Wagner, M. S.; Castner, D. G.; Ratner, B. D.; Horbett, T. A. *J. Biomater. Sci., Polym. Ed.* **2002**, *13*, 367−390.
(6) Harris, J. M. In *Poly(ethylene glycol) Chemistry: Biotechnical and Biomedical Applications*, 2nd ed.; Harris, J. M., Ed.; Plenum Press: New York, 1992; pp 1−12.
(7) Krsko, P.; Libera, M. *Mater. Today* **2005**, *8*, 36−44.
(8) Peppas, N. A. In *Biomaterials Science: An Introduction to Materials in Medicine*, 2nd ed.; Ratner, B. D.; Hoffman, A. S.; Schoen, F. J.; Lemons, J. E., Eds.; Elsevier Academic Press: Amsterdam, 2004; pp 100−107.
(9) Gölander, C. G.; Herron, J. N.; Lim, K.; Claesson, P.; Stenius, P.; Andrade, J. D. In *Poly(ethylene glycol) Chemistry: Biotechnical and Biomedical Applications*, 2nd ed.; Harris, J. M., Ed.; Plenum Press: New York, 1992; pp 221−245.
(10) Sharma, S.; Popat, K. C.; Desai, T. A. *Langmuir* **2002**, *18*, 8728−8731.
(11) Bergstrom, K.; Holmberg, K.; Safranj, A.; Hoffman, A. S.; Edgell, M. J.; Kozlowski, A.; Hovanes, B. A.; Harris, J. M. *J. Biomed. Mater. Res., Part A* **1992**, *26*, 779−790.
(12) Malmsten, M.; Emoto, K.; Van Alstine, J. M. *J. Colloid Interface Sci.* **1998**, *202*, 507−517.
(13) Ko, Y. G.; Kim, Y. H.; Park, K. D.; Lee, H. J.; Lee, W. K.; Park, H. D.; Kim, S. H.; Lee, G. S.; Ahn, D. J. *Biomaterials* **2001**, *22*, 2115−2123.
(14) Meyerbröker, N.; Li, Z. A.; Eck, W.; Zharnikov, M. *Chem. Mater.* **2012**, *24*, 2965−2972.
(15) Harder, P.; Grunze, M.; Dahint, R.; Whitesides, G. M.; Laibinis, P. E. *J. Phys. Chem. B* **1998**, *102*, 426−436.
(16) Papra, A.; Gadegaard, N.; Larsen, N. B. *Langmuir* **2001**, *17*, 1457−1460.
(17) Ma, H. W.; Li, D. J.; Sheng, X.; Zhao, B.; Chilkoti, A. *Langmuir* **2006**, *22*, 3751−3756.
(18) Ma, H. W.; Wells, M.; Beebe, T. P.; Chilkoti, A. *Adv. Funct. Mater.* **2006**, *16*, 640−648.
(19) Larsson, A.; Ekblad, T.; Andersson, O.; Liedberg, B. *Biomacromolecules* **2007**, *8*, 287−295.
(20) Ekblad, T.; Bergstroem, G.; Ederth, T.; Conlan, S. L.; Mutton, R.; Clare, A. S.; Wang, S.; Liu, Y. L.; Zhao, Q.; D'Souza, F.; Donnelly, G. T.; Willemsen, P. R.; Pettitt, M. E.; Callow, M. E.; Callow, J. A.; Liedberg, B. *Biomacromolecules* **2008**, *9*, 2775−2783.
(21) Groll, J.; Amirgoulova, E. V.; Ameringer, T.; Heyes, C. D.; Rocker, C.; Nienhaus, G. U.; Moeller, M. *J. Am. Chem. Soc.* **2004**, *126*, 4234−4239.
(22) Groll, J.; Ameringer, T.; Spatz, J. P.; Moeller, M. *Langmuir* **2005**, *21*, 1991−1999.
(23) Ameringer, T.; Hinz, M.; Mourran, C.; Seliger, H.; Groll, J.; Moeller, M. *Biomacromolecules* **2005**, *6*, 1819−1823.
(24) Groll, J.; Fiedler, J.; Engelhard, E.; Ameringer, T.; Tugulu, S.; Klok, H. A.; Brenner, R. E.; Moeller, M. *J. Biomed. Mater. Res., Part A* **2005**, *74A*, 607−617.
(25) Chen, R. T.; Marchesan, S.; Evans, R. A.; Styan, K. E.; Such, G. K.; Postma, A.; McLean, K. M.; Muir, B. W.; Caruso, F. *Biomacromolecules* **2012**, *13*, 889−895.
(26) Andreopoulos, F. M.; Beckman, E. J.; Russell, A. J. *Biomaterials* **1998**, *19*, 1343−1352.
(27) Montaguea, M.; Ducker, R. E.; Chong, K. S. L.; Manning, R. J.; Rutten, F. J. M.; Davies, M. C.; Leggett, G. J. *Langmuir* **2007**, *23*, 7328−7337.
(28) Ahmad, S. A.; Hucknall, A.; Chilkoti, A.; Leggett, G. J. *Langmuir* **2010**, *26*, 9937−9942.
(29) Jeyachandran, Y. L.; Terfort, A.; Zharnikov, M. *J. Phys. Chem. C* **2012**, *116*, 9019−9028.
(30) Ballav, N.; Thomas, H.; Winkler, T.; Terfort, A.; Zharnikov, M. *Angew. Chem., Int. Ed.* **2009**, *48*, 5833−5836.
(31) Eck, W.; Craig, G.; Sigdel, A.; Ritter, G.; Old, L. J.; Tang, L.; Brennan, M. F.; Allen, P. J.; Mason, M. D. *ACS Nano* **2008**, *2*, 2263−2272.
(32) Matsuura, M.; Miyazawa, T. *J. Polym. Sci., Part B: Polym. Phys.* **1969**, *7*, 1735−1744.
(33) Ratner, B. D.; Castner, D. G. In *Surface Analysis: The Principal Techniques*, 2nd ed.; Vickerman, J. C.; Gilmore, I. S., Eds.; Wiley & Sons: Chichester, U.K., 2009; pp 47−83.
(34) Seah, M. P.; Dench, W. A. *Surf. Interface Anal.* **1979**, *1*, 2−11.
(35) Toomey, R.; Freidank, D.; Ruhe, J. *Macromolecules* **2004**, *37*, 882−887.
(36) Tanaka, T.; Fillmore, D. J. *J. Chem. Phys.* **1979**, *70*, 1214−1218.
(37) Ghosh, S. K.; Pal, T. *Chem. Rev.* **2007**, *107*, 4797−862.
(38) Ung, T.; Liz-Marzan, L. M.; Mulvaney, P. *Colloids Surf., A* **2002**, *202*, 119−126.
(39) Tokarev, I.; Tokareva, I.; Minko, S. *Adv. Mater.* **2008**, *20*, 2730−2724.
(40) Holland, W. R.; Hall, D. G. *Phys. Rev. Lett.* **1984**, *52*, 1041−1044.
(41) Leitner, A.; Zhao, Z. S.; Brunner, H.; Aussenegg, F. R.; Wokaun, A. *Appl. Opt.* **1993**, *32*, 102−110.
(42) Aussenegg, F. R.; Brunner, H.; Leitner, A.; Lobmaier, C.; Schalkhammer, T.; Pittner, F. *Sens. Actuators, B* **1995**, *29*, 204−209.